



# Hierarchical assemblies of $\text{Cd}_x\text{Zn}_{1-x}\text{S}$ complex architectures and their enhanced visible-light photocatalytic activities for $\text{H}_2$ -production



Jian Wang<sup>a,b</sup>, Bo Li<sup>a,c</sup>, Jiazang Chen<sup>a,b</sup>, Li Li<sup>a</sup>, Jianghong Zhao<sup>a</sup>, Zhenping Zhu<sup>a,\*</sup>

<sup>a</sup> State Key Laboratory of Coal Conversion, Institute of Coal Chemistry, Chinese Academy of Sciences, Taoyuan South Road 27, Taiyuan, 030001 Shanxi, People's Republic of China

<sup>b</sup> University of Chinese Academy of Sciences, Beijing 100039, People's Republic of China

<sup>c</sup> College of Chemistry and Chemical Engineering, Lanzhou University, Lanzhou 730000, People's Republic of China

## ARTICLE INFO

### Article history:

Received 6 April 2013

Received in revised form 1 July 2013

Accepted 2 July 2013

Available online 11 July 2013

### Keywords:

$\text{Cd}_x\text{Zn}_{1-x}\text{S}$

Hierarchical architectures

Photocatalytic

Hydrogen evolution

## ABSTRACT

The shape-controlled synthesis of hierarchically micro- and nanostructured materials has opened up new opportunities to improve their properties. In this work,  $\text{Cd}_x\text{Zn}_{1-x}\text{S}$  complex architectures, such as microflowers and microspheres, were prepared through a facile solvothermal method, by using diethylenetriamine (DETA) and water as solvent. Within the Zn content increase from 0.2 to 0.8 in the  $\text{Cd}_x\text{Zn}_{1-x}\text{S}$  solid solution, the morphology transformed progressively from microflowers agglomerates to microspheres. The photocatalytic  $\text{H}_2$  evolution over the solid solutions was further investigated through the  $\text{H}_2$  evolution from aqueous solutions containing  $\text{S}^{2-}/\text{SO}_3^{2-}$ , and the highest  $\text{H}_2$  evolution rate without co-catalysts even reached  $1.8 \text{ mmol g}^{-1} \text{ h}^{-1}$ . The reasons for the difference in the photocatalytic properties of these  $\text{Cd}_x\text{Zn}_{1-x}\text{S}$  architectures were also investigated. The morphology change of  $\text{Cd}_x\text{Zn}_{1-x}\text{S}$  solid solution leads to different BET and surface defects, finally resulting in the variation of photocatalytic activity.

© 2013 Elsevier B.V. All rights reserved.

## 1. Introduction

Since the pioneering work by Fujishima and Honda, heterogeneous photocatalytic water splitting over inorganic semiconductor catalysts for  $\text{H}_2$  evolution has attracted considerable attention [1]. However, most of the developed photocatalyst with wide band gap can only absorb the ultraviolet light. To maximize the use of solar energy, visible light-responsive semiconductor photocatalysts should be developed [2–4]. As an important semiconductor, cadmium sulfide ( $\text{CdS}$ ) nanocrystals has the narrow band-gap ( $E_g = 2.4 \text{ eV}$ ) and valence bands at relatively negative potentials, which make it suitable for hydrogen production under visible light in the presence of sacrifice agents [5–7]. Nevertheless, the photocatalytic efficiency of  $\text{CdS}$  for water splitting is still limited, it is necessary to find suitable method for its structure modification. One strategy is to incorporate of  $\text{ZnS}$  into the structure of  $\text{CdS}$  for forming the series of  $\text{Cd}_x\text{Zn}_{1-x}\text{S}$  solid solution with adjustable band-gap [8,9], its conduction band and valence band can shift to more positive and negative position, leading to the increment of photocatalytic properties [10,11].

It is well known that the applications for materials depend critically on their properties such as the crystal structure, size, shape, specific area and surface defect states. For improving the

photocatalytic activity, it is very important to synthesize the nanocrystals with a specific size and morphology. To date,  $\text{Cd}_x\text{Zn}_{1-x}\text{S}$  compounds with different morphologies, including nanoparticles [12] and rod-like nanostructures [13,14], have been prepared and used as catalysts in photocatalytic systems. And it has been found that these photocatalysts have better photocatalytic  $\text{H}_2$ -production activities. Recently, some hierarchical micro- and nanostructured materials composed of nanosized building blocks such as nanoparticles or nanorods have been prepared and found to have new properties and exhibit potential applications in photocatalytic fields [15–17]. For example, some semiconductors such as  $\text{Fe}_2\text{O}_3$  [18],  $\text{ZnO}$  [19], and  $\text{TiO}_2$  [20] with a hierarchical structure were successfully synthesized and exhibited well photocatalytic properties. However, there is no research on the photocatalytic water splitting for hydrogen production by using the complex hierarchical  $\text{Cd}_x\text{Zn}_{1-x}\text{S}$  micro- and nanostructure.

In the current study, a series of  $\text{Cd}_x\text{Zn}_{1-x}\text{S}$  solid solutions with hierarchical structures have been efficiently synthesized in a DETA aqueous solution through a one-step mix-solvothermal method. The photocatalytic performance was then evaluated through the  $\text{H}_2$  evolution from aqueous solutions containing  $\text{S}^{2-}/\text{SO}_3^{2-}$  under visible light irradiation ( $\lambda > 420 \text{ nm}$ ). The  $\text{Cd}_{0.2}\text{Zn}_{0.8}\text{S}$  microspheres exhibited the best photocatalytic activity with  $\text{H}_2$  production rate of ca.  $1.8 \text{ mmol g}^{-1} \text{ h}^{-1}$ , probably resulted from the needful surface area and surface defect. After loading 1 wt.% Pt on the surface of  $\text{Cd}_{0.2}\text{Zn}_{0.8}\text{S}$ , the rate of  $\text{H}_2$  production even can reach  $5 \text{ mmol g}^{-1} \text{ h}^{-1}$ .

\* Corresponding author. Tel./fax: +86 351 4048433.

E-mail address: [zpzh@sxicc.ac.cn](mailto:zpzh@sxicc.ac.cn) (Z. Zhu).

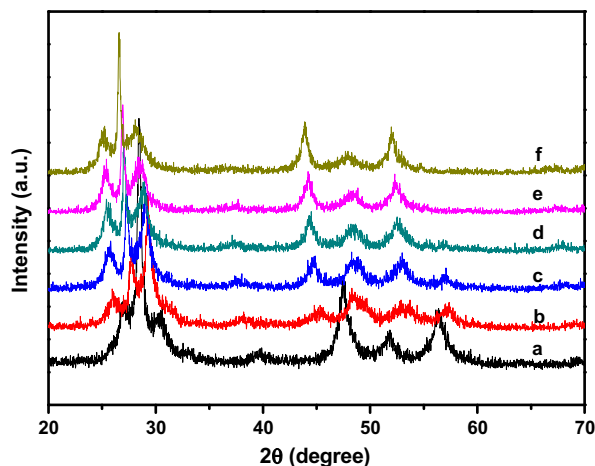


Fig. 1. The XRD pattern for  $Cd_xZn_{1-x}S$  nanocrystals: (a) ZnS (b)  $Cd_{0.2}Zn_{0.8}S$  (c)  $Cd_{0.4}Zn_{0.6}S$  (d)  $Cd_{0.6}Zn_{0.4}S$  (e)  $Cd_{0.8}Zn_{0.2}S$  and (f) CdS.

## 2. Experimental

### 2.1. $Cd_xZn_{1-x}S$ nanocrystal syntheses

The chemicals used in this study were all analytical reagent grade and used without further purification. The  $Cd_xZn_{1-x}S$  nanocrystals were prepared through a solvothermal route. First, a suitable amount of  $Cd(CH_3COOH)_2 \cdot 2H_2O$  and  $Zn(CH_3COOH)_2 \cdot 2H_2O$  (total amount of  $Cd^{2+}$  and  $Zn^{2+} = 10$  mmol) and 20 mmol thiourea were dissolved in 24 mL deionized water. DETA (12 mL) was then added into the aqueous solution. The mixture was stirred to form a homogeneous solution and placed in an autoclave with an inner Teflon lining (the volume is 50 mL). Then the autoclaves were maintained at 180 °C for 12 h and cooled to room temperature. Finally, the product was filtered, washed several times with distilled water and ethanol, and dried in a vacuum oven at 60 °C for 12 h.

### 2.2. Characterization

The X-ray diffraction (XRD) patterns were obtained using a Bruker D8 Advance X-ray diffractometer (Germany) with  $Cu K\alpha$  radiation. The UV–Vis absorption spectra were obtained using a Shimadzu UV–Vis–NIR spectrophotometer (UV-3600, Japan). Photoluminescence (PL) spectra were recorded at room temperature on a fluorescence spectrophotometer (Hitachi F-7000, Japan) using Xenon lamps as the excitation source, all samples were excited using a wavelength of 300 nm. Scanning electron microscopy (SEM) was conducted using a LEO-438VP field emission scanning electron microscope (Germany). Transmission electron microscopy (TEM) was performed using a JEM-2100 transmission electron microscope (Japan) using a 200 kV accelerating voltage. The Brunauer–Emmett–Teller (BET) surface area were measured by a nitrogen adsorption technique at 77 K using an ASAP2020M automated gas-sorption system (America).

### 2.3. Photocatalytic $H_2$ production on the $Cd_xZn_{1-x}S$ solid solution

The photocatalytic reaction was conducted in a closed glass circulation system. The  $Cd_xZn_{1-x}S$  photocatalyst (0.1 g) was dispersed in a 100 mL aqueous solution containing 0.1 M  $Na_2S$  and 0.1 M  $Na_2SO_3$ , which served as sacrificial agents. Pt was in situ photodeposited from the  $H_2PtCl_6 \cdot 6H_2O$  precursor to act as a co-catalyst for the promotion of  $H_2$  evolution. The entire reaction process was irradiated using a 300 W Xe lamp (Trustech PLS-300UV, China) with a cutoff filter ( $\lambda \geq 420$  nm). The amount of  $H_2$  evolved was determined using an online thermal conductivity detector (TCD) gas chromatograph with Ar as the carrier gas.

Table 1

The lattice constants and band gap of  $Cd_xZn_{1-x}S$  solid solution.

Catalyst		CdS	$Cd_{0.8}Zn_{0.2}S$	$Cd_{0.6}Zn_{0.4}S$	$Cd_{0.4}Zn_{0.6}S$	$Cd_{0.2}Zn_{0.8}S$	ZnS
Lattice	$a$ (Å)	4.1187	4.0916	4.0625	4.0525	4.0439	3.7826
Constants	$c$ (Å)	6.6868	6.6674	6.6426	6.6194	6.5804	6.5526
Band gap (eV)		2.11	2.21	2.29	2.37	2.45	3.45

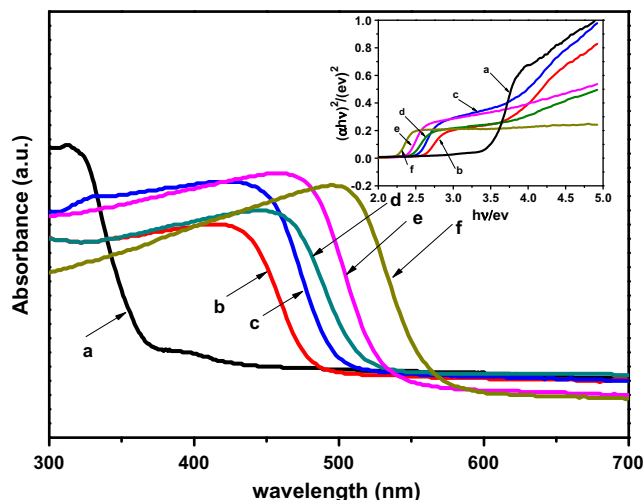


Fig. 2. The UV–Vis spectrum for  $Cd_xZn_{1-x}S$  nanocrystals: (a) ZnS (b)  $Cd_{0.2}Zn_{0.8}S$  (c)  $Cd_{0.4}Zn_{0.6}S$  (d)  $Cd_{0.6}Zn_{0.4}S$  (e)  $Cd_{0.8}Zn_{0.2}S$  and (f) CdS.

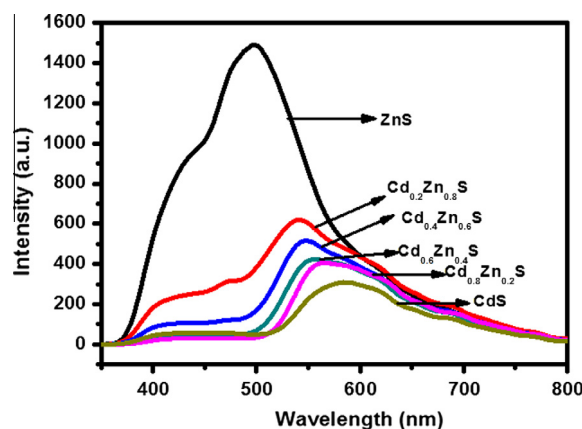
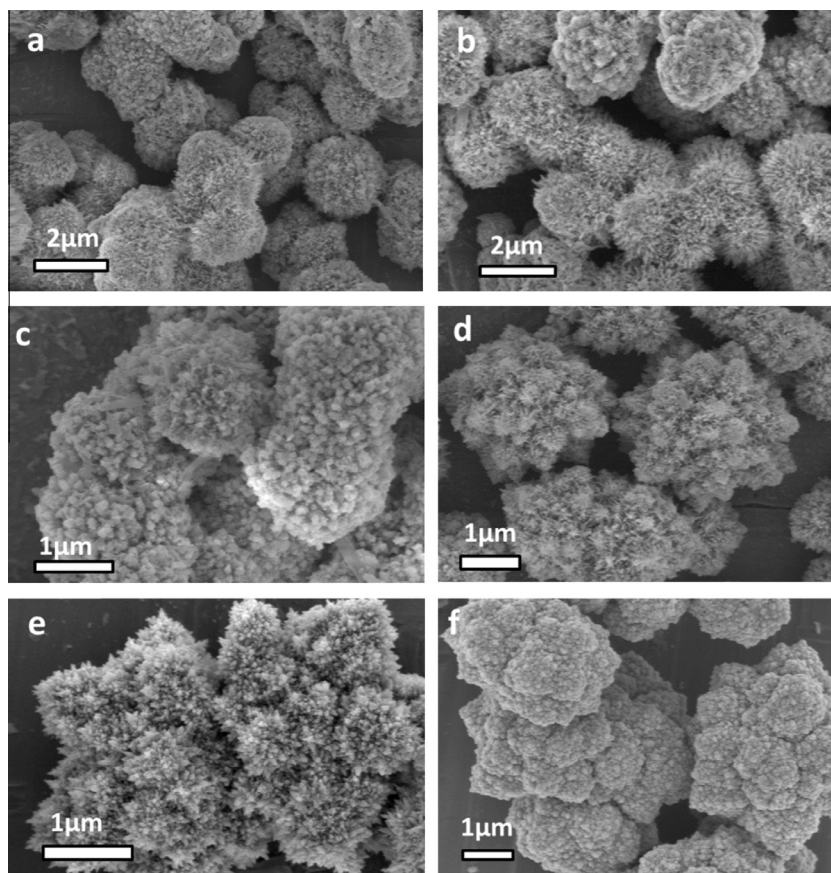


Fig. 3. The PL spectrum for  $Cd_xZn_{1-x}S$  nanocrystals.

## 3. Results and discussion

### 3.1. Formation of $Cd_xZn_{1-x}S$ solid solutions

XRD was used to characterize the phase structure of the samples. From the Fig. 1, the patterns for CdS and ZnS match well with the standard spectra (JCPDS 41-1049 and 36-1450, respectively). And all of the samples exhibits a pure hexagonal wurtzite structure, with the prominent diffraction peaks corresponding to (100), (002), (101), (110), (103) and (112) planes. Due to the smaller Zn atomic radius than Cd atomic radius, the zinc atoms into CdS crystal cell can form infinite solid solution. And it has been proved that the diffraction peaks of  $Cd_xZn_{1-x}S$  solid solution can shift to lower angles as the value of  $x$  in the  $Cd_xZn_{1-x}S$  solid solution increases [12,13]. In our experimental, the diffraction peak also changes with different Cd and Zn composition, indicating



**Fig. 4.** The scanning electron microscopy of  $\text{Cd}_x\text{Zn}_{1-x}\text{S}$  nanocrystals: (a) ZnS (b)  $\text{Cd}_{0.2}\text{Zn}_{0.8}\text{S}$  (c)  $\text{Cd}_{0.4}\text{Zn}_{0.6}\text{S}$  (d)  $\text{Cd}_{0.6}\text{Zn}_{0.4}\text{S}$  (e)  $\text{Cd}_{0.8}\text{Zn}_{0.2}\text{S}$  and (f) CdS.

the successful synthesis of  $\text{Cd}_x\text{Zn}_{1-x}\text{S}$  solid solution. The lattice constants  $a$  and  $c$  for hexagonal phase of  $\text{Cd}_x\text{Zn}_{1-x}\text{S}$  solid solutions was calculated using the following equation:

$$\frac{1}{d^2} = \frac{4}{3} \left( \frac{h^2 + hk + k^2}{a^2} \right) + \frac{l^2}{c^2}$$

The calculated lattice constants  $a$  and  $c$  are listed in Table 1. The changes of lattice constants also demonstrate the formation of solid solutions.

The UV–Vis absorption spectra of the  $\text{Cd}_x\text{Zn}_{1-x}\text{S}$  solid solutions with different Cd concentrations are shown in Fig. 2. The absorption edge of ZnS is approximately 370 nm, but the other samples exhibit intense absorption bands with steep edges in the visible light region. In addition, the absorption edge of the  $\text{Cd}_x\text{Zn}_{1-x}\text{S}$  solid solution gradually red-shifts as the amount of Cd increase. This phenomenon can be attributed to a band transition rather than a transition from impurity levels, indicating the formation of the  $\text{Cd}_x\text{Zn}_{1-x}\text{S}$  solid solution. In view of the direct band gap nature of  $\text{Cd}_x\text{Zn}_{1-x}\text{S}$ , the relation between the absorption coefficient ( $\alpha$ ) and incident photon energy ( $h\nu$ ) can be written as  $\alpha h\nu = C(h\nu - E_g)^{1/2}$ , where  $C$  is a constant and  $E_g$  is the direct band gap. Hence, the band gap value of  $\text{Cd}_x\text{Zn}_{1-x}\text{S}$  architectures can be obtained through extrapolating the linear part of the  $(h\nu) - (\alpha h\nu)^2$  plot to  $(\alpha h\nu)^2 = 0$  (Inset Fig. 2). The specific band gap data can be shown in Table 1. The band gap for CdS is a little lower than the reported data ( $E_g$  of ca. 2.47 eV) and the reason may be that the aggregation in the sample results in large particle sizes, leading to enhanced light harvesting and red-shifted light absorption.

For the further study of the optical properties samples, photoluminescence (PL) measurement was measured at room temperature. Fig. 3 shows the PL spectrum of  $\text{Cd}_x\text{Zn}_{1-x}\text{S}$  solid solution at

an excitation wavelength of 280 nm. It can be found the ZnS has a strong broad emission at 428 nm. Similarly, the PL spectrum of CdS also has a strong emission at 581 nm. The near band edge (NBE) emissions of both ZnS and CdS do not correspond to their absorption wavelength, inferring that the PL is commonly attributed to the recombination of the charge carriers within the surface states. And for the  $\text{Cd}_x\text{Zn}_{1-x}\text{S}$  solid solution, it can also be speculated from the PL spectrum that the luminescence emissions are similarly derived from the surface defect states. Moreover, the intensity of the strongest emission peak increases as Zn component, suggesting the increases of surface defects.

### 3.2. $\text{Cd}_x\text{Zn}_{1-x}\text{S}$ alloy nanocrystal morphology

Since preparing the materials in nanoscale dimension is one of the significant methods to improve the photocatalytic activity, the morphology of  $\text{Cd}_x\text{Zn}_{1-x}\text{S}$  was investigated through SEM and TEM. Fig. 4 shows the SEM images of the synthesized  $\text{Cd}_x\text{Zn}_{1-x}\text{S}$  samples. The pure ZnS nanocrystals clearly consist of microspheres which were stacked by short nanorods. Under solvothermal conditions, the structures and morphologies of ZnS nanostructures have been studied in DETA or in an aqueous DETA solution [21]. With the increases of water and decreases of DETA, the morphologies of ZnS will transfer from nanosheets to microsphere. In our experimental, the volume of water and DETA is 2:1; the synthetic ZnS microspheres conformed to this rule. However, the morphologies of CdS were microflowers that assembled from nanorods. CdS microflowers can also be produced in a mixed solution of DETA and deionized water via a facile solvothermal approach [22]. With decreasing the volume of DETA and water, the CdS microflowers would be formed. In our experimental, the morphologies of CdS may be associated with it. As the solid solution is formed, the

formed nanocrystals with different morphologies that depend on the Zn content of the solid solutions. The nanocrystals made of microflowers have a low Zn content ( $x = 0.2$  or  $0.4$ ), but the microspheres would be found in the high Zn content ( $x = 0.2$  or  $0.4$ ) samples. Similar  $Cd_xZn_{1-x}S$  nanocrystals have been prepared by using  $(NH_4)_2S$  as sulfur source in a mixed solution of DETA and water [23]. The possible reason for the morphology change may be the difference of the  $M^{2+}$  ion ( $M = Zn^{2+}$  or  $Cd^{2+}$ ) reactivity with  $S^{2-}$ , which follows the order,  $Cd^{2+} > Zn^{2+}$ . More the detailed is needed further investigation. The morphologies of  $Cd_xZn_{1-x}S$  solid solution was also characterized by TEM (shown in Fig. S1), the similar morphology change rule can be associated to the SEM results.

In order to further analyze the basic assembled units, the  $Cd_{0.2}Zn_{0.8}S$  sample was taken as an example to do HRTEM and selected-area electron diffraction (SAED) characterization. Fig. S2a shows the HRTEM images of the synthesized  $Cd_xZn_{1-x}S$  samples, the clear lattice fringe indicates the products have high crystallization and single crystal properties. And the clear-cut 0.33 nm lattice spacing can be corresponding to the wurtzite (002) plane. Some structural deformations are also found in the HRTEM which can be duo to the elemental default or asymmetric doping. The corresponding selected-area electron diffraction (SAED, Fig. S2b) pattern indicates that the typical  $Cd_{0.2}Zn_{0.8}S$  sample has a hexagonal single-crystal structure. These results show that  $Cd_{0.2}Zn_{0.8}S$  preferentially grew along the (001) direction.

### 3.3. Photocatalytic performance of the $Cd_xZn_{1-x}S$ solid solution

The photocatalytic performance of the  $Cd_xZn_{1-x}S$  solid solution in  $H_2$  production was investigated in a system consisting of 0.1 M  $Na_2S$ /aqueous  $Na_2SO_3$  solution. Fig. 5a shows that all the  $Cd_xZn_{1-x}S$  photocatalysts exhibit high activities than that of ZnS and CdS, indicating that the formation and composition of the solid solution is significant for  $H_2$  production. In particular, the  $Cd_{0.2}Zn_{0.8}S$  microsphere exhibits the best activity among the  $Cd_xZn_{1-x}S$  solid solutions, with a  $H_2$  production rate of  $\sim 1.8 \text{ mmol g}^{-1} \text{ h}^{-1}$ , which is almost 30 times higher than that of CdS. Moreover, the rate of  $H_2$  production for  $Cd_xZn_{1-x}S$  decreases as the Cd concentration in the solid solution increases, suggesting the composition for solid solution has an important impact on the photocatalytic activities. In the same test conditions, the photocatalytic  $H_2$ -production activity of hierarchical  $Cd_xZn_{1-x}S$  complex architectures is better than the reported nanoparticles [24–27].

During the photocatalytic water splitting process, co-catalysts like noble metals are often needed to promote the separation of photogenerated carriers and provide low activation potentials for  $H_2$  evolution, thus serving as active sites for  $H_2$  production. For the CdS and  $Cd_xZn_{1-x}S$  solid solution photocatalyst, noble metal such as Pt, Pd and Rh were studied as co-catalysts to enhance the photocatalytic activity, and Pt has showed the most favorable effect on the improvement of CdS photocatalytic activity. When Pt is loaded into the  $Cd_xZn_{1-x}S$  photocatalysts, the photocatalytic activity further increases. The rate of  $H_2$  evolution over the Pt/ $Cd_{0.2}Zn_{0.8}S$  photocatalyst reaches as high as  $\sim 5 \text{ mmol g}^{-1} \text{ h}^{-1}$  (Fig. 5b), which is approximately 1.8 times higher than that over the  $Cd_{0.2}Zn_{0.8}S$  solid solution catalyst alone.

The  $Cd_xZn_{1-x}S$  solid solution with a hexagonal wurtzite phase often has the best photocatalytic activity when the Zn content ( $1-x$ ) is approximately 0.6–0.7, which may be attributed to the suitable band gap and negative shift of the conduction band. In the current results, the  $Cd_{0.4}Zn_{0.6}S$  solid solution gives a very high rate of  $H_2$  production ( $\sim 0.8 \text{ mmol g}^{-1} \text{ h}^{-1}$ ), most probably because of the aforementioned reason. However, the  $Cd_{0.2}Zn_{0.8}S$  solid solution exhibits the best photoactivity for  $H_2$  production. Therefore, aside from the band-gap structure for the hierarchical  $Cd_xZn_{1-x}S$  solid solution, other influence factors should be considered.

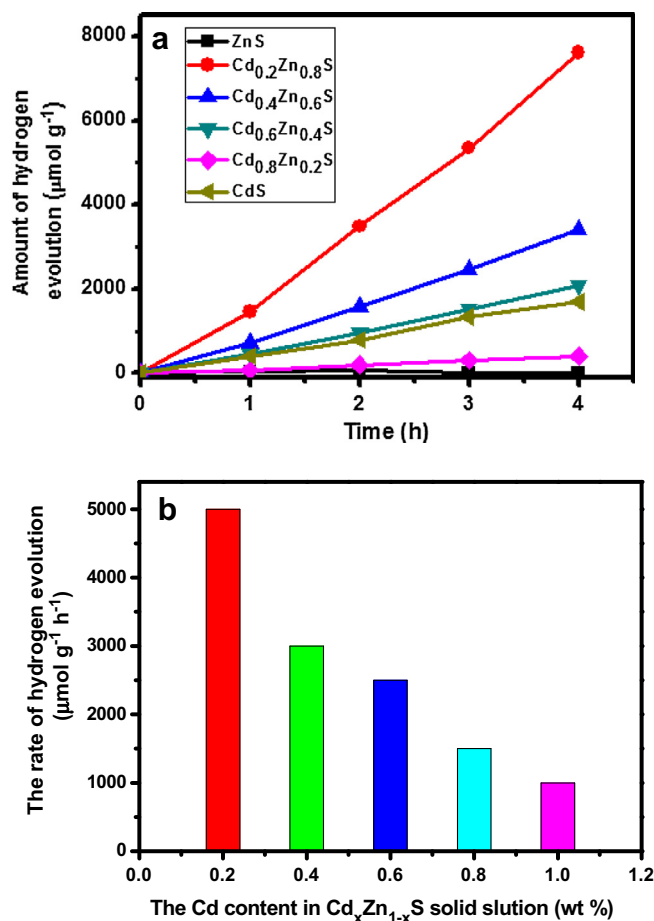


Fig. 5. (a) Hydrogen evolution of different  $Cd_xZn_{1-x}S$  solid solution photocatalysts in  $Na_2SO_3$  and  $Na_2S$  aqueous solutions (Catalyst: 0.1 g, light source: 300 W Xe lamp with a cutoff filter ( $\lambda \geq 420 \text{ nm}$ )) (b) Hydrogen evolution of different  $Cd_xZn_{1-x}S$  loading with 1 wt.% Pt as co-catalyst in  $Na_2SO_3$  and  $Na_2S$  aqueous solutions.

When photons with sufficient energy strike the semiconductor photocatalyst, they create pairs of electrons and holes, then the electron–hole pairs would be separated, transferred into the surface of catalyst and reacted with water, so the surface properties such as BET surface areas and surface defects have an great effect on the photocatalytic activities. In general, the bigger the specific area of semiconductor, the more of active sites with reactants, which is helpful for photocatalytic reaction. Conversely, it is unfavorable to the photocatalytic reaction. At the same time, the surface defects also have important influence on the catalytic activity. The suitable surface defects have a help to capture photo-generated electronic or hole, leading more electron or hole to migrate to the surface of the catalyst for photocatalytic reaction.

The synthetic hierarchical assemblies of  $Cd_xZn_{1-x}S$  complex architectures have different morphology. In particular, the morphology changes from microflowers agglomerates to microspheres with the Cd content in the solid solution, which may generate changes of surface properties. Firstly, the BET of  $Cd_xZn_{1-x}S$  solid solution has been changed. As shown in Table 2, the ZnS has a relatively high BET data ( $\sim 40 \text{ m}^2/\text{g}$ ), and the CdS exhibits low surface area, only  $7 \text{ m}^2/\text{g}$ . For the different constituent solid solution, the BET data will increase with the Cd content decrease, and the  $Cd_{0.2}Zn_{0.8}S$  microsphere especially has a higher BET results ( $\sim 42 \text{ m}^2/\text{g}$ ). Apparently, the higher BET is in favor of providing more reaction site, causing the enhancement of photocatalytic activity. In addition, the change of  $Cd_xZn_{1-x}S$  morphologies is also possible for

**Table 2**  
The BET of  $\text{Cd}_x\text{Zn}_{1-x}\text{S}$  solid solution.

Catalyst	CdS	$\text{Cd}_{0.8}\text{Zn}_{0.2}\text{S}$	$\text{Cd}_{0.6}\text{Zn}_{0.4}\text{S}$	$\text{Cd}_{0.4}\text{Zn}_{0.6}\text{S}$	$\text{Cd}_{0.2}\text{Zn}_{0.8}\text{S}$	ZnS
BET ( $\text{m}^2/\text{g}$ )	7	22	26	36	42	40

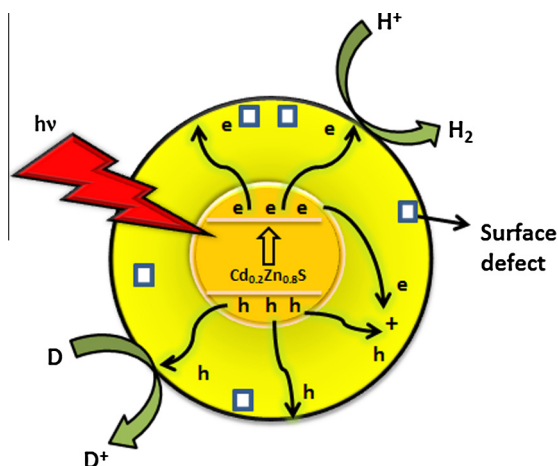


**Fig. 6.** Schematic illustration of  $\text{Cd}_x\text{Zn}_{1-x}\text{S}$  in photocatalytic processes.

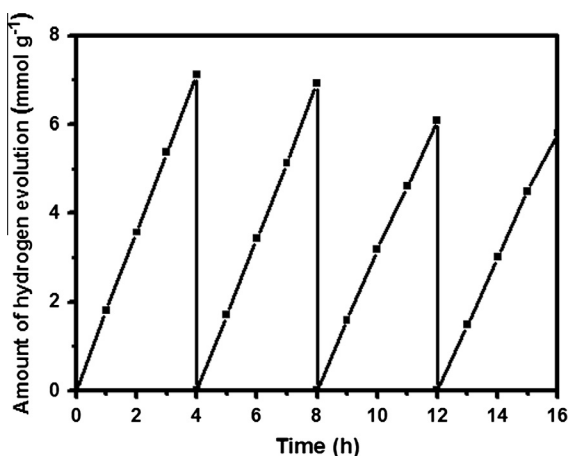
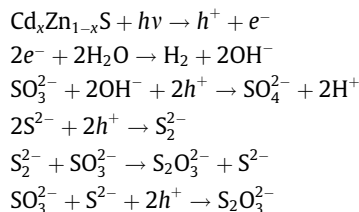


**Fig. 7.** Amounts of  $\text{H}_2$  evolution according to reaction time of  $\text{Cd}_{0.2}\text{Zn}_{0.8}\text{S}$ .

the difference of surface defect. From the PL spectrum (Fig. 3), it can be seen that the  $\text{Cd}_{0.2}\text{Zn}_{0.8}\text{S}$  has the strongest PL emission peak, implying there is more surface defect state as the electronic reservoir to improve the photocatalytic activity. In the reported literatures, through the modification of the surface defects of  $\text{Cd}_x\text{Zn}_{1-x}\text{S}$  nanocrystals,  $\text{Cd}_{0.2}\text{Zn}_{0.8}\text{S}$  also exhibits the highest rate of photocatalytic  $\text{H}_2$ -production [28]. Based on the above analysis, the  $\text{Cd}_{0.2}\text{Zn}_{0.8}\text{S}$  solid solution with the best photoactivity for  $\text{H}_2$  production can be explained by Fig. 6. When the  $\text{Cd}_{0.2}\text{Zn}_{0.8}\text{S}$  photocatalyst absorbs the visible light, its suitable band position makes it have a stronger driver force for water reduction. Meanwhile, the specific morphology can absorb lots of water molecules. And the numbers of surface defect states play the role of electron pool to promote the separation of the charge carriers in photocatalysis, thus leading to the improvement of photocatalytic activity.

The stability of catalyst is also important in the photocatalytic process. A typical reaction time course of  $\text{H}_2$  evolution over  $\text{Cd}_{0.2}\text{Zn}_{0.8}\text{S}$  photocatalyst was also shown in Fig. 7. The reaction system

was evacuated after each run. By combination of  $\text{SO}_3^{2-}$  and  $\text{S}^{2-}$  utilized as sacrificial agent, different reactions occurred for the photoexcited holes as follows:



Therefore, no significant decrease in the photocatalytic activity is observed, the hydrogen evolution rate still reached and  $1.6 \text{ mmol g}^{-1} \text{ h}^{-1}$  in the fourth reaction run.

#### 4. Conclusions

A series of hierarchical  $\text{Cd}_x\text{Zn}_{1-x}\text{S}$  micro- and nanostructure have been synthesized in a DETA and water solution using the solvothermal method. The morphology of the nanoflowers was characterized. Within the Zn content increase from 0.2 to 0.8 in the  $\text{Cd}_x\text{Zn}_{1-x}\text{S}$  solid solution, the morphology transformed progressively from microflowers agglomerates to microspheres. Furthermore, the photocatalytic performance of the  $\text{Cd}_x\text{Zn}_{1-x}\text{S}$  nanoflowers in  $\text{H}_2$  evolution was investigated. The  $\text{Cd}_{0.2}\text{Zn}_{0.8}\text{S}$  solid solution composed of thin slices exhibited the best photocatalytic activity for  $\text{H}_2$  evolution, with an initial rate of  $1.8 \text{ mmol g}^{-1} \text{ h}^{-1}$ . This high activity may be due to the specific morphology which has a relatively high BET and surface defects, leading to a high number of reaction sites.

#### Acknowledgments

The authors are grateful for the financial support of the Knowledge Innovation Project of Chinese Academy of Sciences (No. KJCX2.YW.M10).

#### Appendix A. Supplementary material

Supplementary data associated with this article can be found, in the online version, at <http://dx.doi.org/10.1016/j.jallcom.2013.07.013>.

#### References

- [1] A. Fujishima, K. Honda, *Nature* 238 (1972) 37–38.
- [2] X. Chen, S. Shen, L. Guo, S.S. Mao, *Chem. Rev.* 110 (2010) 6503–6570.
- [3] A. Kudo, Y. Miseki, *Chem. Soc. Rev.* 38 (2009) 253–278.
- [4] R.M. Navarro Yerga, M.C. Álvarez Galván, F. del Valle, J.A. Villoria de la Mano, J.L.G. Fierro, *ChemSusChem* 2 (2009) 471–485.
- [5] N. Bao, L. Shen, T. Takata, K. Domen, *Chem. Mater.* 20 (2007).
- [6] M. Sathish, R.P. Viswanath, *Catal. Today* 129 (2007) 421–427.
- [7] H. Yan, J. Yang, G. Ma, G. Wu, X. Zong, Z. Lei, J. Shi, C. Li, *J. Catal.* 266 (2009) 165–168.
- [8] Y.C. Li, M.F. Ye, C.H. Yang, X.H. Li, Y.F. Li, *Adv. Funct. Mater.* 15 (2005) 433–441.
- [9] Y. Liu, J.A. Zapfen, Y.Y. Shan, C.Y. Geng, C.S. Lee, S.T. Lee, *Adv. Mater.* 17 (2005) 1372–1377.
- [10] F. del Valle, A. Ishikawa, K. Domen, J.A. Villoria de la Mano, M.C. Sánchez-Sánchez, I.D. González, S. Herreras, N. Mota, M.E. Rivas, M.C. Álvarez Galván, J.L.G. Fierro, R.M. Navarro, *Catal. Today* 143 (2009) 51–56.
- [11] C. Xing, Y. Zhang, W. Yan, L. Guo, *Int. J. Hydrogen Energy* 31 (2006) 2018–2024.
- [12] W.Z. Wang, W. Zhu, H.L. Xu, *Monodisperse, J. Phys. Chem. C* 112 (2008) 16754–16758.
- [13] S. Biswas, S. Kar, S. Santra, Y. Jompol, M. Arif, S.I. Khondaker, *J. Phys. Chem. C* 113 (2009) 3617–3624.
- [14] W. Li, D. Li, W. Zhang, Y. Hu, Y. He, X. Fu, *J. Phys. Chem. C* 114 (2010) 2154–2159.
- [15] L.-S. Zhong, J.-S. Hu, A.-M. Cao, Q. Liu, W.-G. Song, L.-J. Wan, *Chem. Mater.* 19 (2007) 1648–1655.

- [16] Y. Li, J. Liu, X. Huang, G. Li, *Cryst. Growth Des.* 7 (2007) 1350–1355.
- [17] C. Gu, J. Huang, Y. Wu, M. Zhai, Y. Sun, J. Liu, *J. Alloys Comp.* 509 (2011) 4499–4504.
- [18] L. Han, Y. Chen, Y. Wei, *CrystEngComm* 14 (2012) 4692–4698.
- [19] B. Li, Y. Wang, *J. Phys. Chem. C* 114 (2009) 890–896.
- [20] G. Tian, Y. Chen, W. Zhou, K. Pan, C. Tian, X.-r. Huang, H. Fu, *CrystEngComm* 13 (2011) 2994–3000.
- [21] W.T. Yao, S.H. Yu, L. Pan, J. Li, Q.S. Wu, L. Zhang, J. Jiang, *Small* 1 (2005) 320–325.
- [22] W.-T. Yao, S.-H. Yu, S.-J. Liu, J.-P. Chen, X.-M. Liu, F.-Q. Li, *J. Phys. Chem. B* 110 (2006) 11704–11710.
- [23] Y. Chen, X. Zhang, C. Jia, Y. Su, Q. Li, *J. Phys. Chem. C* 113 (2009) 2263–2266.
- [24] W. Zhang, Z. Zhong, Y. Wang, R. Xu, *J. Phys. Chem. C* 112 (2008) 17635–17642.
- [25] D.-H. Wang, L. Wang, A.-W. Xu, *Nanoscale* 4 (2012) 2046–2053.
- [26] G.J. Liu, L. Zhao, L.J. Ma, L.J. Guo, *Catal. Commun.* 9 (2008) 126–130.
- [27] X.H. Zhang, D.W. Jing, M.C. Liu, L.J. Guo, *Catal. Commun.* 9 (2008) 1720–1724.
- [28] J. Shi, J. H.n. Cui, J. Z. Liang, J. X. Lu, J. Y. Tong, J. C. Su, J. H. Liu, *Energy Environ. Sci.* 4 (2011) 466–470.